Journal of The Electrochemical Society, **154** (2) B147-B152 (2007)
0013-4651/2006/154(2)/B147/6/$20.00 © The Electrochemical Society

Isothermal Cold Start of Polymer Electrolyte Fuel Cells

Kazuya Tajiri, Yuichiro Tabuchi,[a] and Chao-Yang Wang*,z

Electrochemical Engine Center (ECEC) and Department of Mechanical and Nuclear Engineering, The Pennsylvania State University, University Park, Pennsylvania 16802, USA

Experimental procedures, aimed at elucidating fundamentals of polymer electrolyte fuel cell startup from subzero temperatures, are reported. A method of equilibrium purge using partially humidified gas with well-controlled relative humidity is introduced to effectively control initial water distribution inside a cell prior to cold start. Isothermal cold start, in which single cells with sufficiently large thermal mass are used to fix the cell temperature constant at the startup ambient temperature, is proposed to study intrinsic cold start capability of the membrane-electrode assembly. The proton conductivity of membranes with low water content and at subzero temperatures is measured in situ. The cumulative product water in mg/cm^2 has been used to quantify performance of isothermal cold start and is shown to exhibit a nonlinear relationship with the membrane water uptake potential, defined as the difference between the membrane hydration water content and initial value prior to cold start. It is found that the membrane is a key component to enhance the intrinsic capability of isothermal cold start from −30°C. Finally, when the current density is high, the pore volume of the cathode catalyst layer is not fully utilized for ice storage, thereby decreasing cold start performance.
 [DOI: 10.1149/1.2402124]

Manuscript submitted August 14, 2006; revised manuscript received September 26, 2006.
Available electronically December 15, 2006.

Cold start capability and survivability of polymer electrolyte fuel cells (PEFCs) in a subzero environment remains a challenge for automotive applications. Fundamental mechanisms are not fully determined, but it is recognized that product water becomes ice or frost upon startup when the PEFC internal temperature is below the freezing point of water. If the local pore volume of the cathode catalyst layer (CL) is insufficient to contain all of the accumulated water before the operating temperature of the cell rises above freezing, the solid water may plug the CL and stop the electrochemical reaction by starving the reactant gases.

Very little is known about the physical nature of PEFC cold start, and despite its importance to fuel cell deployment, there is limited active research in this area (albeit there exist a large number of system-based patents that do not necessarily address basic questions).[1-13] Initial studies of McDonald et al.[1] and Cho et al.[2,3] focused on thermal cycling between room temperature and a subzero temperature. That is, no electrochemical reaction or water production occurred in these systems under subzero temperatures. Cho et al.[2] studied the effect of thermal cycle between 80 and −10°C on a wet polymer membrane, and found that cell performance drastically degraded after only four cycles, and that various characteristics of the membrane-electrode assembly (MEA), such as its pore size distribution and cyclic voltammograms, were changed. In a later study, Cho et al.[3] observed that purging the cell with dry gas or filling the cell compartments with an antifreeze solution before the cell temperature drops below 0°C can prevent MEA degradation. McDonald et al.[1] also found that temperature dependence of the proton conductivity of Nafion 112 membrane does not change in slope, indicating that no phase transition of water within the membrane and no CL degradation occur, for dry MEA subject to freeze-thaw cycling between −40 and 80°C. Limited information on MEA degradation from cold start cycles in which electrochemical reaction and water production occur at subzero temperatures was provided by Mao et al.[4] Notably, this work revealed interfacial delamination between the membrane and cathode catalyst layer after 110 cycles of cold start at 500 mA/cm^2 by transmission electron microscopy (TEM), but no such delamination was found in the same MEA from 110 cycles of cold start at 100 mA/cm^2.

Kagami et al.[6] and Hishinuma et al.[7] explored the cold start performance of a 104 cm^2 single cell both experimentally and numerically, and concluded that self-startup of a PEFC below −5°C was impossible without external heat assist. Oszcipok et al.[8] conducted potentiostatic discharge experiments of a PEFC and fitted statistically the cumulative charge-transfer density before cell shutdown with the air flow rate during startup and membrane water content prior to startup. In these experiments the cell was purged with dry nitrogen until the cell resistance increased by a factor of 100 or more before cool down and cold start. Subsequently, Oszcipok et al.[9] experimentally studied the effects of membrane thickness, gas diffusion layer (GDL), and gas flow rates on the cumulative charge-transfer density.

Using visualization images obtained from an operating PEFC, Ge and Wang[10] investigated liquid water transport prior to freezing and ice-frost formation after freezing directly on the surface of the CL. An important conclusion drawn from this work is that the freezing-point depression of water in the cathode CL is no greater than 2°C and plays a negligible role in cold start theory and practice.

Clearly, much remains to be done to establish both engineering fundamentals of PEFC startup from subzero temperatures and basic understanding of associated MEA degradation. The present study reports on a set of experimental protocols for cold start research that uses laboratory-scale single cells. Aimed at generating reproducible and consistent data that are indicative of intrinsic cold start capability of MEA and other key components rather than highly dependent on cell fixtures, the present experimental procedures consist of equilibrium gas purge and isothermal cold start until cell shutdown, as will be elaborated below.

Equilibrium purge.— Gas purge is a common and integral part of PEFC cold start in the industry. The primary purpose of gas purge is to remove residual water from a PEFC prior to cell shutdown and cool down. The gas purge process thus defines the initial condition of water distribution throughout a cell and plays a crucial role in cold start. While commonly gas purge is conducted using dry nitrogen/air for durations ranging from tens of seconds to a few minutes, in this work we introduce a method using partially humidified gas with well-controlled relative humidity (RH) to purge for extended periods of time (of the order of several hours). After this purge, all liquid water should be evaporated away from all components of the cell and the membrane water content reaches thermodynamic equilibrium with the RH of purge gas (thus termed equilibrium purge). Equilibrium purge permits the initial water content in the membrane to be precisely controlled and well defined (through the RH control in purge gas) and, hence, the important effect of the initial water distribution on cold start performance can be studied, as will be illustrated in this paper.

* Electrochemical Society Active Member.
[a] On leave from Nissan Motor Co. Ltd.
[z] E-mail: cxw31@psu.edu

Isothermal cold start.— In practice, cold start of a PEFC stack is inherently nonisothermal, as power generation produces waste heat that causes the cell temperature to rise. However, nonisothermal cold start data vary greatly from one system to another and strongly depend on the thermal mass of the test cell-stack. For the purposes of determining key MEA characteristics to ensure self-startup of an automotive PEFC from, e.g., −30°C and ultimately to relate these characteristics to materials and control requirements, isothermal cold start is uniquely useful as proposed here. Isothermal cold start can be easily realized in laboratories by using a single cell fixture with sufficiently large thermal mass. While isothermal cells (the cell temperature is always kept constant at the ambient temperature of startup) are bound to shut down, the product water so measured before cell shutdown is a quantitative measure of the intrinsic cold start capability of an MEA that is completely independent of the thermal mass of a specific cell. Such experimental data are therefore of benchmark quality, highly reproducible in laboratories (independent of cell fixtures), and practically useful for stack design as the amount of product water also roughly corresponds to the amount of waste heat able to be generated. Last, isothermal cold start provides the most conservative scenario to examine the impacts of MEA materials and designs on performance of PEFC cold start.

Intuitively, the performance of PEFC cold start is measured by how long a cell can operate before it is shut down by ice filling in the cathode CL. However, we propose to use the total product water (in the unit of mg/cm^2) to quantify the cold start performance for reasons that product water: (*i*) combines the effects of current density and operational time; (*ii*) allows direct comparison with water accumulation in various components such as the membrane, CL, and GDL; and (*iii*) is indicative of the amount of waste heat generated from the cell according to the following derivation

$$\text{Heat generation (J/cm}^2) = \int (E_h - V_{\text{cell}}) I dt \approx (E_h - V_{\text{cell}}) \int I dt = \frac{2F(E_h - V_{\text{cell}})}{M_{\text{H}_2\text{O}}} m_{\text{H}_2\text{O}} \quad [1]$$

where E_h is the thermal potential ($=\Delta h/2F \sim 1.48$ V for H_2–O_2 reaction), V_{cell} the operating cell voltage in cold start (assumed to be roughly constant, e.g., at 0.6 V), $M_{\text{H}_2\text{O}}$ the molecular weight of water, and $m_{\text{H}_2\text{O}}$ the total product water in mg/cm^2 generated from cold start. That is

$$m_{\text{H}_2\text{O}} = \frac{M_{\text{H}_2\text{O}}}{2F} \int I dt \quad [2]$$

From Eq. 1 the amount of waste heat capable of generating from a cell during cold start can be easily estimated from the product water, and subsequently the stack temperature rise can be computed by dividing the waste heat by the thermal mass of the stack.

Experimental

Experimental setup.— The test cell used in this study has 25 cm^2 active area with both anode and cathode flow fields consisting of straight, parallel channels. The bipolar plates (BP) are made of graphite with the total thickness of 15 mm. Two pairs of gold-plated copper current collectors of 4 mm thickness and stainless-steel end plates of 15 mm thickness are placed outside the two graphite BPs. The heat capacitance of these components per unit active area is about 20 J/cm^2 K, resulting in a maximum temperature increase of ~0.1°C for 1 min of operation at 0.5 V and 40 mA/cm^2, if in the absence of any heat loss to the ambient. The MEAs used in this study are commercially available Japan Gore-Tex MEAs with 30 μm thick membrane and CL with Pt loading of 0.4 mg/cm^2 on each electrode. Toray carbon paper coated with a microporous layer (MPL) was used as the GDL.

The experimental setup is shown schematically in Fig. 1. For all experiments carried out at temperatures above the freezing point,

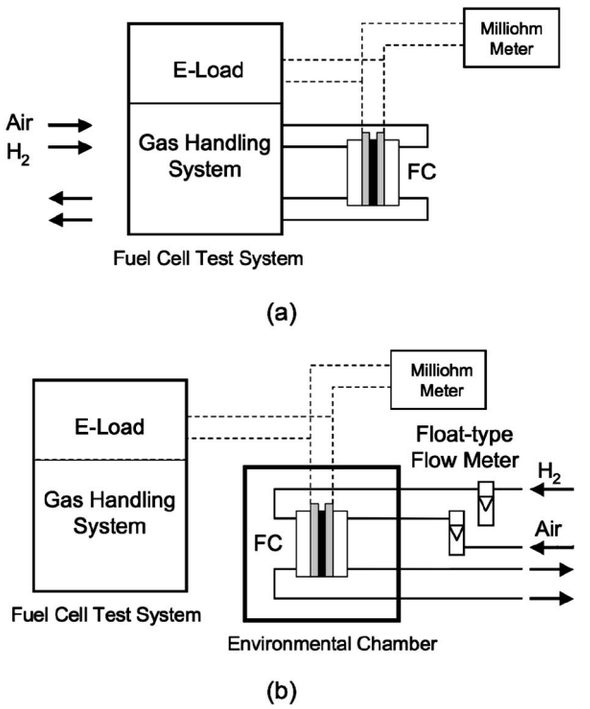

Figure 1. Experimental setup for (a) operation above the freezing temperature, and (b) startup from a subfreezing temperature.

Arbin fuel cell test system (Arbin Instruments, College Station, TX) is used to control the load, cell temperature, and anode and cathode gas parameters such as flow rate, dew point, and back-pressure (see Fig. 1a). For cold start experiments performed inside a subzero environmental chamber as shown in Fig. 1b, dry hydrogen and air directly from gas bottles are fed into the cell with separate rotameters to control their flow rates in order to avoid entrainment of any water vapor from humidifiers of the fuel cell test station.

To simulate the cold ambient temperature, the test cell is placed in a Tenney environmental chamber (model T10C; Lunaire Limited, Williamsport, PA). The chamber is precooled from the room temperature to a prescribed startup temperature such as −30°C, and about 2 h are required for the test cell to reach −30°C after being placed in the chamber.

In addition to recording voltage-time curves during constant current density startup, cell resistance is measured and monitored by a Tsuruga milliohm meter (model 3566; Osaka, Japan). The meter is operated at 7.4 mA of ac current with 1 kHz frequency. The high-frequency resistance (HFR) data, along with cell temperature recorded by thermocouples, are logged by an Agilent 34970A data acquisition unit (Agilent Technologies, Inc., Loveland, CO) on a PC.

Procedure.— The procedure for all cold start experiments reported in this work consists of four steps: cell conditioning, gas purge, cool down, and startup, as described in detail below.

The test cell is first conditioned by operation at the current density of 500 mA/cm^2 and 55°C for 30 min. Both anode and cathode gases are kept at 100% RH, and the H_2 and air flow rates are 1.57 and 4.48 L/min, respectively.

As mentioned earlier, the method of equilibrium purge is developed in this experimental work to initialize the cell internal condition before each cold start experiment. In this process the fuel cell temperature and the gas dew point are set to prescribed values, and nitrogen gases are supplied to both anode and cathode channels. The purge process continues until the cell HFR measured by the milliohm meter reaches a final, stabilized value. At this point in time it is considered that the MEA reaches equilibrium with the purge gas

Table I. Experimental conditions for equilibrium purge.

Case no.	Cell Temperature (°C)	Gas Dew Point (°C)	Relative Humidity (%)	Membrane Water Content
1	60	30	21	2.4
2	50	30	34	2.9
3	35	30	75	6.2
4	30	30	100	14.0

RH, and residual liquid water in the CL and GDL pores or gas channels is completely removed. Under this condition the water content of the MEA can be easily calculated from the purge gas RH via the membrane water uptake curve such as[14]

$$\lambda = 0.043 + 17.81a - 39.85a^2 + 36.0a^3$$

where λ is the water content in the membrane and a is the relative humidity of the purge gas. Typically the equilibrium purge takes 2 to 3 h to complete.

In this study the dew point of the purge gas is fixed at 30°C while the cell temperature during purge varies at 30, 35, 50, and 60°C so as to create a RH range of 21 to 100% and corresponding water content in the membrane at 2.4, 2.9, 6.2, and 14. All equilibrium purge cases and their conditions are summarized in Table I.

The third step in a cold start experiment is cool down of the fuel cell. Once equilibrium purge is concluded, the inlet and outlet gas lines are closed for both anode and cathode in order to keep the cell internal condition unchanged, and the cell is then moved inside the environmental chamber. In the chamber the fuel cell temperature and the cell resistance are simultaneously measured during cool down. When the cell temperature reaches a specified startup temperature, the cell is left at that temperature for more than 1 h before proceeding to the next step in order to ensure that the entire cell becomes isothermal at the ambient temperature. In the present work the test cell is cooled down and started up at −30°C, as this is the most challenging startup temperature required for automotive application.

During cooldown, water content in the membrane can be safely assumed to remain constant or "locked" in place. This assumption can be justified by the fact that the cell compartment on each side has about 2 cm^3 and its filling gas at the dew point of 30°C after equilibrium purge contains ~0.06 mg of water, equivalent to an increase in membrane water content of $\Delta\lambda = 0.02$. Thus, the change in membrane water content during cool down is negligible, making it possible to predetermine the membrane water content at the beginning of cold start.

The final step involves operating the test cell under a subfreezing temperature. After dry reactant gases are supplied to the cell and the open-circuit voltage rises, a given current density is applied from the Arbin fuel cell test system. The current density applied increases linearly from zero at the rate of 0.5 $mA/cm^2/s$ for 80 s and then is kept constant at 40 mA/cm^2, unless otherwise specified. When the voltage drops below a preset cutoff voltage (i.e., 0.3 V in the present study), the load is released and the cold start experiment is terminated. The total product water from each cold start experiment can be calculated from the total operational time and the applied current density via Eq. 2.

Results and Discussion

The change in cell resistance during equilibrium purge is displayed in Fig. 2 for case 1 listed in Table I. The cell temperature and purge gas dew point are 60 and 30°C, respectively, resulting in purge gas RH of ~21% and water content of 2.4 in the membrane at the end of equilibrium purge. It is seen from Fig. 2 that the membrane resistance rapidly rises in the first 10 min and then slowly increases for the next 2 h. This behavior is consistent with the most recent measurements of liquid water removal from GDL by purge gas using X-ray microtomography.[15] It was found that the water saturation in GDL decreases rapidly in the first 6 min by purge gas, after which this decrease slows substantially between 6 and 25 min.

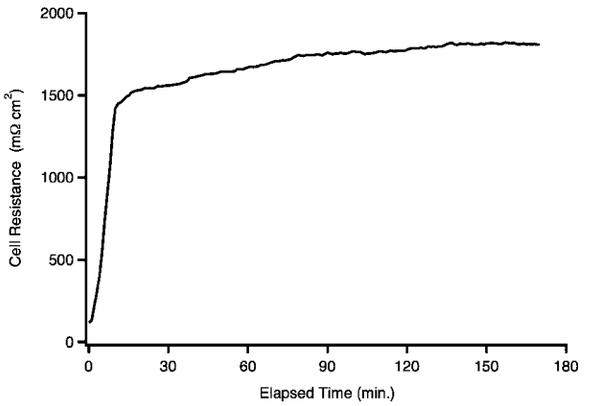

Figure 2. The cell resistance change with time during equilibrium purge at the cell temperature and purge gas dew point of 60 and 30°C, respectively (case 1).

The final stage of removing all liquid water trapped in small pores of CL, MPL, and GDL takes much longer because there is high tortuosity for purge gas to reach these sites for evaporation. This time-consuming stage is required before the membrane fully reaches equilibrium with water vapor in the purge gas, as any small amount of liquid water remaining in porous components will serve as a water reservoir to rehydrate the electrolyte in the CL and membrane. For all cases of equilibrium purge listed in Table I, the overall trend and time scale of HFR vs time curves remain similar.

The cool-down process also provides an opportunity to obtain the membrane proton conductivity as a function of temperature at known water content. Note that the temperature dependence of proton conductivity with low membrane water content is of particular interest here as PEFC cold start rarely involves fully hydrated membranes after gas purge. In addition, unlike PEFCs operated under normal temperatures, the membrane resistance under low water content and low temperature typical of cold start conditions is much greater than the contact resistance, thus making in situ measurements of the membrane proton conductivity in a PEFC a simple but accurate method.

Figure 3 shows the proton conductivity variation with temperature for varying membrane water content. In the Arrhenius form the lines displayed in Fig. 3 are nearly straight and parallel to each other, indicating no noticeable phase transition of water occurring in

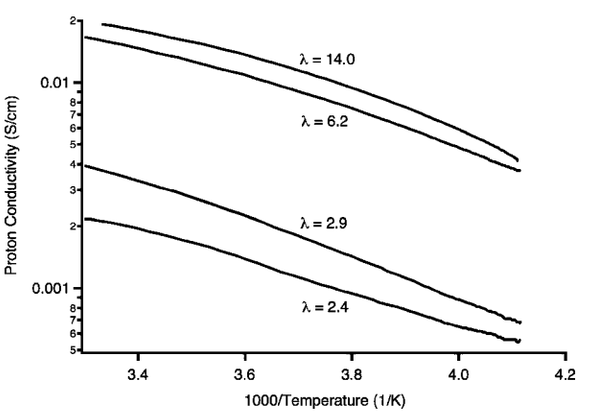

Figure 3. Proton conductivity as a function of temperature for various membrane water content λ between room temperature and −30°C.

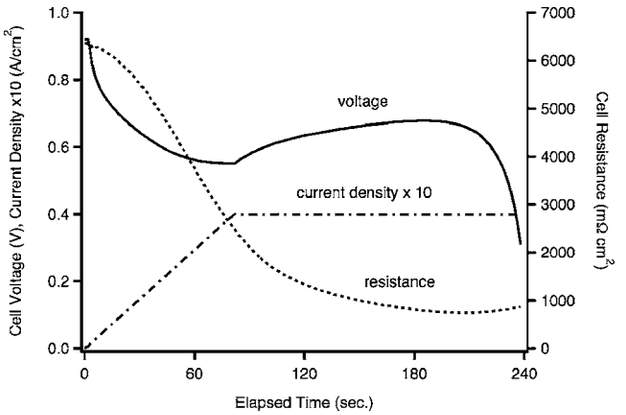

Figure 4. Time evolution of applied current density, cell voltage, and cell resistance during startup from −30°C for case 1 of equilibrium purge.

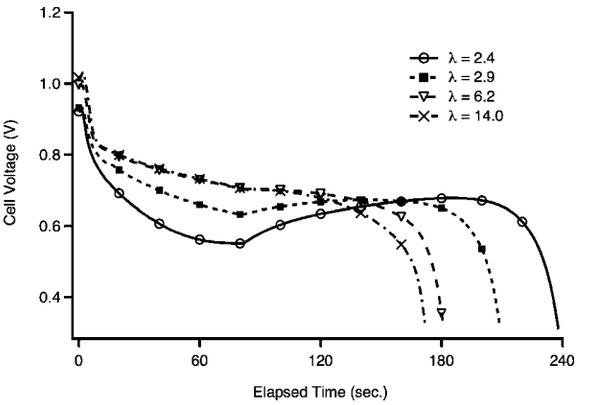

Figure 5. Effect of initial water content λ in the membrane on cold start performance. The environmental temperature is −30°C.

the membrane in this temperature range between room temperature and −30°C and water content range from 2.4 to 14. This finding is in good agreement with observations of McDonald et al.[1] for partially hydrated Nafion 112-based MEAs. For the $\lambda_i = 14$ case, the conductivity curve shown in Fig. 3 is slightly convex. This may be because the 100% RH purge gas used in equilibrium purge could not remove all liquid water by evaporation from the interfaces between GDL and current-collecting lands, or between CL and GDL, resulting in water freezing at these interfaces during cool down and hence a change in contact resistance.

The conductivity data measured in situ in this work are within the temperature range from room temperature (27°C) to −30°C. In contrast, Cleghorn et al. reported the proton conductivity for Gore-Select membranes in the temperature range of 40–100°C.[16] Extrapolating the correlation of Cleghorn et al. to 27°C and at 100% RH, the membrane conductivity is calculated to be 0.027 S/cm, which is in reasonable agreement with our in situ measurement of 0.021 S/cm.

Figure 4 shows the evolution of cell voltage and resistance with time during cold start from −30°C for case 1 of equilibrium purge listed in Table I. The applied current density is an initial ramp of 0.5 mA/cm^2/s for 80 s followed by constant 40 mA/cm^2. The cell voltage initially decreases under the load and as the applied current density increases, then slightly rises until about 3.5 min, after which voltage drop-down is evident until the cutoff voltage of 0.3 V. The cell resistance is seen to decrease during both the initial current ramp and the full load periods, dropping from initially 6000 to 800 mΩ cm^2 at the final stage of cold start. This resistance decrease is direct evidence of gradual absorption of product water generated from CL into the membrane. Owing to membrane rehydration during cold start, the cell voltage recovers a little between 90 and 210 s into the cold start, as can be seen from Fig. 4. The iR-free (internal resistance-free) voltage is computed to change from 650 to 710 mV in this voltage recovery period, which indicates that there may also be a slight improvement in activation besides the membrane resistance reduction. The rapid voltage drop in the final stage of cold start is apparently due to hindrance of oxygen transport into an ice-filled CL. The product water generated from oxygen reduction reaction (ORR) is difficult to remove from CL via vapor phase transport because of the very low saturation vapor pressure (P_{sat} = 40 Pa at −30°C). Consequently, product water accumulates in the cathode CL unless it partially diffuses into the membrane. Notice also that water existing in CL under isothermal cold start from −30°C, as involved in the present experiments, must be in the form of ice or frost according to the freezing-point depression observations made by Ge and Wang.[10]

The effect of initial membrane water content prior to cold start on the voltage curve during cold start is shown in Fig. 5. During the initial current ramp period the cell voltage is higher as the initial membrane water content increases, as expected. In the voltage recovery period two characteristics can be noticed. First, the voltage recovery due to membrane rehydration decreases as the initial membrane water content increases. Second, the duration of this period is greater for lower initial water content. For the $\lambda_i = 14$ case the voltage recovery is hardly seen and the profile moves directly from the initial period to the final voltage drop-down stage. This is because the membrane is already nearly saturated at the beginning of cold start and hence no room remains to accommodate product water diffusion. Consequently, the total operational time of cold start discharge increases as the initial membrane water content decreases, demonstrating the profound significance of gas purge.

In light of the importance of water storage in partially dry membranes, it is instructive to correlate the cold start performance quantified by product water (m_{H_2O},mg/cm^2) with the membrane water uptake potential ($\Delta\lambda$) defined as

$$\Delta\lambda = \lambda_{sat} - \lambda_i \quad [3]$$

where λ_{sat} denotes the water content of a fully hydrated membrane (taken to be 14 in this study) and λ_i the initial membrane water content prior to cold start. If a membrane is initially fully hydrated prior to cold start, i.e., $\lambda_i = \lambda_{sat}$, then the water uptake potential in the membrane is zero, and all product water must accumulate in the CL at the startup temperature of −30°C. If gas purge is highly effective and the membrane is dry initially, then the water uptake potential reaches the maximum, thus resulting in more product water. Figure 6 displays such an experimental relationship between product water and membrane water uptake potential. In the case of $\Delta\lambda = 0$ (i.e., $\lambda_i = 14$) the majority of product water resides in the cathode CL. Thus, the measured product water (i.e., ~0.5 mg/cm^2) in this condition is indicative of the water storage capacity in the CL. One can quickly estimate the latter by the following equation

$$m_{CL} = \delta_{CL}(\varepsilon\rho_{ice} + \varepsilon_e c_{f,dry}\Delta\lambda M_{H_2O}) \quad [4]$$

where the first term on the right-hand side accounts for ice storage in open pores of the CL and the second term for water storage in the electrolyte phase. Assuming typical CL properties (δ_{CL} = 12 μm, ε = 0.5, ρ_{ice} = 0.9 g/cm^3, ε_e = 0.2, and $c_{f,dry}$ = 1.818 × 10^{-3} mol/cm^3), the CL water storage capacity is estimated to be 0.54 mg/cm^2 for $\Delta\lambda = 0$, which is in good agreement with the measured product water. This analysis further suggests that the vapor phase transport of product water out of CL into GDL is indeed negligible at the startup temperature of −30°C.

Figure 6 also shows that the total product water can be separated into the CL and membrane contributions for each water uptake potential in the membrane. While the CL contribution depends mainly on the CL pore volume and weakly on the water uptake potential $\Delta\lambda$

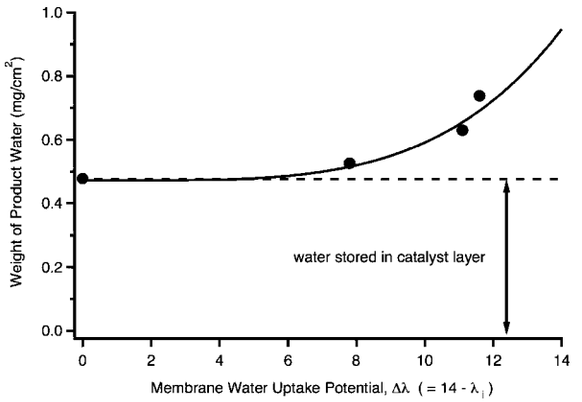

Figure 6. Relation between product water and membrane water uptake potential for the startup from −30°C. The dashed line indicates the amount of water stored in the catalyst layer and the extra portion above it denotes the amount of water diffused into the membrane.

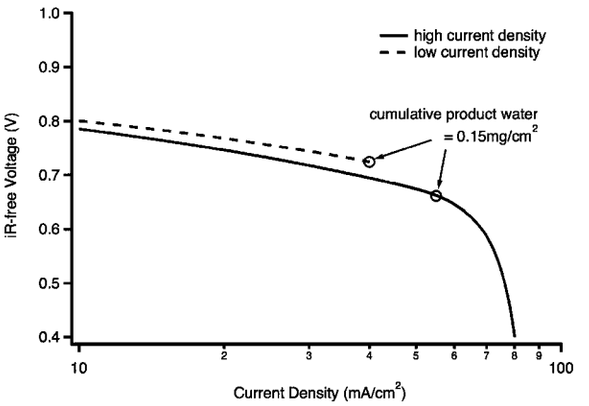

Figure 8. Current-voltage curves with linear scan in current at −30°C for case 3 of equilibrium purge.

as indicated in Eq. 4, the membrane contribution varies nonlinearly with Δλ. This is because longer CL operation before ice filling and shutdown allows more membrane water uptake.

A fundamental map like Fig. 6 is useful for developing MEA materials and designs in order to enhance the intrinsic capability of PEFC cold start. For example, in order to earn more time for product water diffusion into the membrane, low water production rate or current density is preferred for isothermal cold start from startup temperatures as low as −20 or −30°C. This conclusion implied from Fig. 6 can be experimentally verified as discussed below.

To see the effect of the startup current density, the current density profile applied to the cell is doubled. As seen from Fig. 7, the current density is initially increased from 0 to 80 mA/cm^2 with the scan rate of 1 mA/cm^2/s for 80 s, and then kept constant at 80 mA/cm^2 until the voltage drops below the cutoff voltage of 0.3 V. The condition of equilibrium purge for this experiment is case 3, i.e., cell temperature and purge gas dew point are 35 and 30°C, respectively. For the higher current density case the cell voltage drops gradually in the first 1 min and then falls into the voltage drop-down period quickly. Soon after the current density reaches 80 mA/cm^2, the voltage drops below 0.3 V and the cold start operation stops. Thus, only two stages of voltage evolution are evident at this higher current density, as compared to the three stages experienced in the lower current density case shown in Fig. 7.

In Fig. 8 the iR-free voltage is plotted against the applied current density during the initial current ramp period of the startup for both current densities. This plot can be viewed as a polarization curve under linear current scan. For the low current density case the iR-free voltage decreases nearly linearly with log(i), indicative of a typical Tafel kinetic behavior of ORR. However, for the higher current density this linear relationship persists only up to ~55 mA/cm^2, and beyond this threshold current density there is appreciable mass transport loss, implying that the limiting step has shifted from the charge-transfer kinetics to mass transport. At this transition point the cumulative product water is found to be 0.15 mg/cm^2. At the same cumulative product water of 0.15 mg/cm^2, the low current density startup has just reached 40 mA/cm^2 and the cell voltage begins to slightly increase (see Fig. 7). This demonstrates that the cumulative product water of 0.15 mg/cm^2 has not resulted in mass transport limitation in the CL due to ice formation in the low current density case. The cumulative product water at cell shutdown is 0.32 and 0.53 mg/cm^2 for the high and low current densities, respectively. Mass transport limitation in CL with lower product water at higher current density can be explained by the water distribution in CL as schematically shown in Fig. 9. For the low current density case (Fig. 9a), the reaction current distribution is more uniform and product water has sufficient time to redistribute uniformly throughout the pores in CL. Thus, the CL water storage capacity can be fully utilized. In the high current density case (Fig. 9b), the reaction current is nonuniform and is determined by a delicate balance between proton conduction through ionomers and O_2 transport through pores of the catalyst layer. Further, the dominance between the two resistances changes with time during cold start; the proton resistance continues to decrease with more water production but ice formation exacerbates the O_2 transport. As a result, the peak reaction current tends to shift toward the CL/GDL interface in favor of O_2 transport, which leads

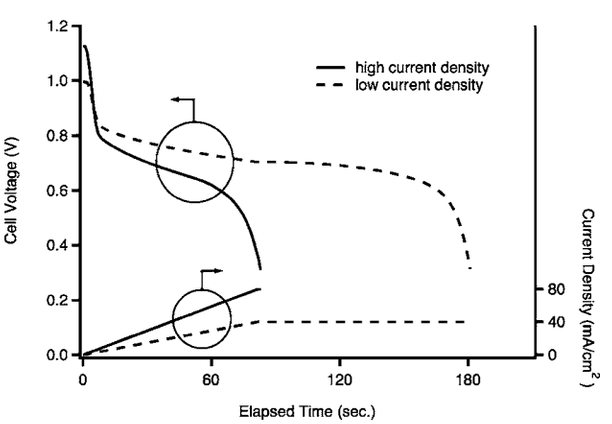

Figure 7. Effect of current density on voltage evolution during cold start from −30°C in case 3 of equilibrium purge.

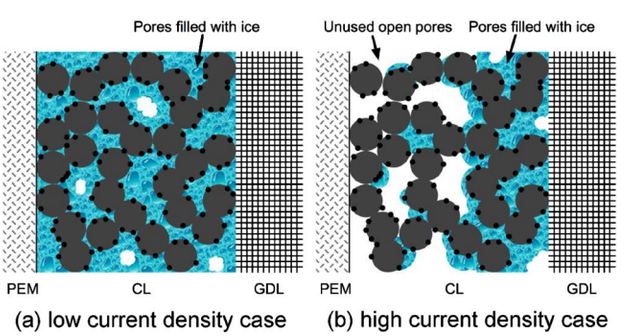

Figure 9. (Color online) Schematic of water distribution at the end of cold start for (a) low current density, and (b) high current density.

to even more ice formation and aggravated mass transport limitation in that region. In addition, product water formed in the CL near the CL/membrane interface is likely to be absorbed in the membrane, leaving less water to precipitate as ice in CL pores. That is, product water may concentrate in the front portion of the electrode interfacing with GDL and form an ice sheet there to block oxygen transport into the CL before all pores are occupied by product water. Thus, the water storage capacity in CL cannot be fully utilized and CL is prematurely shut down under the high current density. The differing utilization in the CL water storage capacity is responsible for ~60% reduction in cold start product water between the high and low current densities.

Using the experimental protocols described above, we have also studied the effects of operating conditions such as startup current density and temperature as well as design parameters such as membrane and catalyst layer thickness. These experimental data are provided elsewhere due to the length limitation of this paper.[11] In addition, the extensive database enabled by the new experimental protocols developed in this work have been employed to successfully validate a multiphase, nonisothermal cold start model.[12,13]

Conclusions

We have introduced the experimental methodologies of equilibrium purge to control the initial water distribution inside a PEFC prior to cold start and isothermal cold start to evaluate the intrinsic startup capability of an MEA from subzero temperatures. Isothermal cold start also provides the most conservative scenario to study impacts of MEA materials and designs on PEFC cold start. The following specific conclusions are drawn from this study.

1. Equilibrium purge can effectively control the cell internal condition before cold start, thereby making consistent and reproducible cold start experiments possible.

2. Proton conductivity in membranes with low water content, typical of cold start conditions, is measured in situ in an operating fuel cell under subzero temperatures. No slope change in the temperature dependence of proton conductivity is found between room temperature and −30°C and for water content between 2.4 and 14, indicative of no phase transition of water occurring in these membranes within the given temperature range.

3. During startup from −30°C, a PEFC with low water content membrane experiences three stages of voltage evolution: an initial drop period under load, a recovery period owing to membrane rehydration by product water and hence lowered membrane resistance, and finally a voltage drop-down due to ice formation in the cathode CL.

4. The amount of product water can be used as a quantitative measure of cold start performance, and it exhibits a nonlinear relationship with the membrane water uptake potential ($\Delta\lambda$).

5. The product water in isothermal cold start from −30°C can be divided into CL and membrane contributions, with the CL contribution principally depending on the CL pore volume and the membrane contribution on water transport through the membrane. Water accumulated in the CL is believed to be ice or frost, and water transport out of CL via vapor phase transport plays a negligible role for cold start from −30°C. Therefore, the membrane is a key component to improve cell performance under isothermal cold start.

6. When the current density is high, the water storage capacity in CL is not fully utilized and, therefore, the total product water decreases.

Acknowledgments

Funding for this work from Nissan Motor Company Limited and Penn State Materials Research Institute is gratefully acknowledged. We also thank Japan Gore-Tex, Incorporated, for providing MEA and Koudai Yoshizawa of Nissan for insightful discussions.

The Pennsylvania State University assisted in meeting the publication costs of this article.

References

1. R. C. McDonald, C. K. Mittelsteadt, and E. L. Thompson, *Fuel Cells*, **4**, 208 (2004).
2. E. A. Cho, J. J. Ko, H. Y. Ha, S. A. Hong, K. Y. Lee, T. W. Lim, and I. H. Oh, *J. Electrochem. Soc.*, **150**, A1667 (2003).
3. E. A. Cho, J. J. Ko, H. Y. Ha, S. A. Hong, K. Y. Lee, T. W. Lim, and I. H. Oh, *J. Electrochem. Soc.*, **151**, A661 (2004).
4. L. Mao, K. Tajiri, S. Ge, X. G. Yang, and C. Y. Wang, Abstract 998, The Electrochemical Society Meeting Abstracts, Vol. 2005-2, Los Angeles, CA, Oct. 16-21, 2005.
5. L. Mao, Ph.D. Thesis, The Pennsylvania State University, University Park, PA (2006).
6. F. Kagami, T. Ogawa, Y. Hishinuma, and T. Chikahisa, in *Fuel Cell Seminar Abstract* (2002).
7. Y. Hishinuma, T. Chikashisa, F. Kagami, and T. Ogawa, *JSME Int. J., Ser. B*, **47**, 235 (2004).
8. M. Oszcipok, M. Zedda, D. Riemann, and D. Geckeler, *J. Power Sources*, **154**, 404 (2006).
9. M. Oszcipok, D. Riemann, U. Kronenwett, M. Kredeweis, and M. Zedda, *J. Power Sources*, **145**, 407 (2005).
10. S. Ge and C. Y. Wang, *Electrochem. Solid-State Lett.*, **9**, A499 (2006).
11. K. Tajiri, Y. Tabuchi, F. Kagami, S. Takahashi, K. Yoshizawa, and C. Y. Wang, *J. Power Sources*, Submitted.
12. L. Mao and C. Y. Wang, *J. Electrochem. Soc.*, **154**, B139 (2006).
13. L. Mao, C. Y. Wang, and Y. Tabuchi, *J. Electrochem. Soc.*, In press.
14. T. E. Springer, T. A. Zawodzinski, and S. Gottesfeld, *J. Electrochem. Soc.*, **138**, 2334 (1991).
15. P. K. Sinha, P. Halleck, and C. Y. Wang, *Electrochem. Solid-State Lett.*, **9**, A344 (2006).
16. S. Cleghorn, J. Kolde, and W. Liu, Chap. 44 in *Handbook of Fuel Cells*, W. Vielstich, A. Lamm, and H. A. Gasteiger, Editors, John Wiley & Sons, New York (2003).